

Check for updates

Plasmonic surface lattice resonances in nanoparticle arrays

Diptesh Dey and George C. Schatz*

This article reviews the literature and provides a detailed computational analysis of the optical properties of one- and two-dimensional arrays of silver and gold nanoparticles, with an emphasis on surface lattice resonances (SLRs) that arise when localized plasmon resonances (LSPRs) in the nanoparticles couple to diffraction resonances that are determined by the interparticle spacing to give polariton modes in which the two types of excitations are coherently coupled. The computations are based on the coupled-dipole approximation, which provides a nearly quantitative description of the extinction spectra for arrays of this type where the particles are well separated and not too large. The computations are used to determine many characteristics of SLRs associated with the lower polariton mode that is mostly photonic in nature, and we also study the upper polariton that is dominated by the LSPR response, as well as Rayleigh anomalies (RAs) that correspond to purely diffractive excitation. The calculations explore the sensitivity of these excitations to the directions of the incident wave and polarization vectors relative to the array axis, the effect of array spacing and number of particles in the array, and the effect of nanoparticle radius and background refractive indices. Details of the physical mechanisms involved in determining blue- and/or redshifts as structural parameters are varied is provided, with SLRs being sensitive to far-field coupling, while LSPRs can also be sensitive to near- and intermediate-field interactions that in some cases are similar to effects found in dye molecule aggregates.

Introduction

Since the pioneering work of Michael Faraday on the colors of colloidal gold particles, there has been considerable experimental and theoretical interest to study the interaction of light with small metallic particles.²⁻⁶ Nanometer-sized metallic particles or structures can strongly absorb or scatter light due to their ability to support plasmon resonances—coherent oscillations of the surface conduction electrons in response to the electric field of light leading to an enhanced optical near-field of subwavelength dimensions.⁷ The local field enhancement is a consequence of the large optical frequency polarization associated with the electron oscillation. If the localization of light takes place within an isolated metal nanostructure, it is termed a localized

surface plasmon resonance (LSPR).8-13 The LSPR frequency of a metallic nanostructure is related to the plasma frequency of the free electrons as determined by the size and shape of the particle and by the permittivity of the metal and the surrounding medium.¹¹ The complex, frequency-dependent dielectric function of a material (also known as the relative permittivity) describes the partial screening of an oscillating electric field within the material, which determines the plasmonic response. Strong particle plasmons result when the real part of the dielectric function (ϵ') is less than zero while the imaginary part (ϵ'') is small and positive. The latter determines the quality of the resonance because it is a measure of the absorption loss. Although dipolar modes usually dominate the optical response, 14

Impact statement

This study describes the optical behavior of one- and two-dimensional arrays of plasmonic silver and gold nanoparticles, based on the coupled-dipole approximation of electrodynamics. A new interpretation is provided for characterizing the optical resonances in such structures, including the identification of both upper and lower polaritons that couple Bragg diffraction modes and localized plasmons. Also, Rayleigh anomalies (Bragg modes not coupled to plasmons) are often but not always present in competition with the lower polariton mode. Connections to strong coupling effects and to plasmonic lasers are briefly discussed.

Diptesh Dey, Department of Chemistry, Northwestern University, Evanston, USA; diptesh.dey@northwestern.edu George C. Schatz, Department of Chemistry, Northwestern University, Evanston, USA; g-schatz@northwestern.edu doi:10.1557/s43577-023-00629-x



higher order modes (quadrupole, octupole) can also contribute.² Since these light-matter interactions are strong and tunable, plasmonic nanoparticles find a wide range of interesting applications that include surface-enhanced Raman scattering, ¹² optical waveguides, and chemical as well as biochemical sensors. 15 To this end, applications of particle plasmons benefit from weak plasmon damping—slow dephasing of the optical polarization associated with the electron oscillation as is especially found for noble metals in the visible and nearinfrared (NIR) region.

When metal nanoparticles are in close proximity, the individual LSPR modes get influenced as the electric near-fields can couple for separations on the order of the particle radius resulting in a new hybrid mode or gap mode—an enhancement of the local electric field in the gap between the particles that causes a shift of the LSPR wavelength. 16-18 On the other hand, for nanoparticles organized into ordered arrays with spacings comparable to the wavelength of light, it is the electric far-field that couples to the diffraction mode of the lattice. This radiative far-field coupling leads to diffractive resonances that are called Rayleigh anomalies (RAs) for dielectric particle arrays, but for plasmonic particle arrays the coupling also leads to polariton formation, and if the RA is to the red of the LSPR, the lower energy polariton is slightly redshifted from the RA (so mostly photonic in character with a narrow width) and its peak extinction (absorption + scattering) and quality factor (Q) are enhanced relative to the LSPR. 19-21 This coherent interaction of plasmon and diffraction arises from multiple scattering by the regularly spaced particles, and the excitation is commonly referred to as a surface lattice resonance (SLR). The terms lattice plasmon polariton or diffractively coupled localized plasmon resonance are also used. 19,22-24 There is also an upper polariton mode that is mostly localized plasmonic in character and hard to distinguish from the properties of isolated nanoparticles, so the polaritonic properties of this mode have rarely been studied (we consider this later), and we will continue to identify this as the LSPR mode of the array. Note that for the lower polariton, the diffractive character of the SLR can lead for 2D arrays to radiation in the plane of the array.²¹ In many cases, the RA manifests itself in the extinction spectrum of the array as a sudden dip just to the blue of the sharp dispersive peak of the SLR, but we will show later that RAs can also show up as peaks rather than dips, and they can sometimes be so close to the SLR that the RA cannot be distinguished in the extinction spectrum. In addition to in-plane excitation, ^{14,25} the radiative coupling and collective resonances that lead to SLRs for 2D arrays can also arise from out-of-plane excitation. 26 Plasmonic SLR modes are therefore very sensitive to the periodicity of the lattice²⁷ and many other properties, leading to interesting optical band structure properties.

Plasmonic SLRs supported by metal nanoparticle arrays have attracted increasing attention in the past two decades by communities involved in both fundamental research and practical applications. ^{21,24,27–30} SLRs find several promising

applications that include nanoscale lasing, 31,32 nonlinear optics³³ and quantum optics. To this end, several researchers have contributed to SLR research. 14,21,24,26,27 Beginning in 2004, Schatz and co-workers have published several theoretical papers concerned with the very sharp SLR resonances for 1D and 2D arrays of metal nanoparticles, ^{19,34–37} and then starting in 2012, Schatz collaborated with Odom and others to connect the theoretical studies to experimental observations, especially those involving the use of SLR in combination with dyes and other emitters to produce SLR lasers. 31,38-42 Significant work by others has also been described, including studies of energy transfer in nanoparticle arrays, studies of Bose-Einstein condensates associated with SLRs, and studies of strong coupling effects involving SLRs and excitons. 43–59 Most of this work has studied silver and gold nanoparticles due to strong plasmon excitation in the visible and NIR, but other metals (copper, aluminum, indium) have also been of interest. 40,57,60

In this Review, we provide theoretical insight on light scattering and absorption from one- and two-dimensional arrays of spherical plasmonic nanoparticles. We consider the coupleddipole method, ^{19,23,24} which provides a semi-analytic approach to interpret the collective optical response using simple concepts. Only dipole (and no higher multipole) polarizabilities are considered to generate coherent excitation of the particles. Much of this work is concerned with determining and interpreting the effects of long-range (radiative) coupling over a range of particle spacings, array structures and incident field directions and polarizations, focusing specifically on 1D and 2D arrays of silver and gold spherical particles. We also consider the influence of array structure and incident light on the properties of the LSPRs and on RAs. While some of this work revisits science that was initially presented nearly 20 years ago, ¹⁹ many new concepts have been developed since then, and there are issues related to polariton properties that are new to this work.

Coupled-dipole method

The coupled-dipole method provides a simple physical picture and an analytic framework to understand the optical response of arrays of nanoparticles. To that end, it involves numerically solving Maxwell's equations to obtain the absorption, scattering, and extinction cross sections for spherical or spheroidal nanoparticles. Each component nanoparticle is assumed to be a dipole resonator of polarizability α_i (for spherical particles) that interacts with the local field at the position of the particle, such that this field is expressed as a sum of the incident plane wave field and the scattered field from the other nanoparticles. The collective optical response of the aggregate is then obtained self-consistently. Since nanoparticles of sizes much smaller than the wavelength of light primarily respond as electric dipoles, higher-order multipole resonances are usually ignored.

Consider an array of N particles whose positions and polarizabilities are denoted by \mathbf{r}_i and α_i , respectively. The induced dipole P_i in each particle in the presence of an



applied plane wave field is $\mathbf{P}_i = \alpha_i \mathbf{E}_{\text{loc},i} (i = 1, 2, ..., N)$, where the local field $\mathbf{E}_{\text{loc},i}$ is the sum of the incident and retarded fields of the other N-1 dipoles. For a given wavelength λ , this field is

$$\mathbf{E}_{\text{loc},i} = \mathbf{E}_{\text{inc},i} + \mathbf{E}_{\text{dipole},i}$$

$$= \mathbf{E}_{0} \exp(i\mathbf{k} \cdot \mathbf{r}_{i}) - \sum_{\substack{j=1\\j \neq i}}^{N} \mathbf{A}_{ij} \cdot \mathbf{P}_{j}, \quad i = 1, 2, ..., N,$$

where \mathbf{E}_0 and $k=2\pi/\lambda$ are the amplitude and wave vector of the incident wave, respectively. The dipole interaction matrix \mathbf{A} is expressed as

$$\mathbf{A}_{ij} \cdot \mathbf{P}_{j} = k^{2} e^{ikr_{ij}} \frac{\mathbf{r}_{ij} \times (\mathbf{r}_{ij} \times \mathbf{P}_{j})}{r_{ij}^{3}}$$

$$+ e^{ikr_{ij}} (1 - ikr_{ij}) \frac{[r_{ij}^{2} \mathbf{P}_{j} - 3\mathbf{r}_{ij}(\mathbf{r}_{ij} \cdot \mathbf{P}_{j})]}{r_{ij}^{5}}$$

$$(i = 1, 2, ..., N, j = 1, 2, ..., N, j \neq i),$$

where \mathbf{r}_{ij} is the vector from dipole *i* to dipole *j*. Note that the first term in Equation 2 has a 1/r dependence on interparticle spacing, while the second has $1/r^2$ and $1/r^3$ variations. As a result, the first term, which is associated with radiative dipolar interactions between the particles, is often dominant for large array spacings.

For a finite array of particles, the polarization vectors are obtained by using iteration to solve 3N linear equations of the form

$$\mathbf{A}'\mathbf{P} = \mathbf{E},$$

where the off-diagonal elements of the matrix \mathbf{A}'_{ij} , \mathbf{A}'_{ij} , are the same as \mathbf{A}_{ij} , and the diagonal elements of the matrix, \mathbf{A}'_{ii} , are α_i^{-1} . For a system of N elements, \mathbf{E} and \mathbf{P} are 3N dimensional vectors, and \mathbf{A}' is a $3N \times 3N$ matrix. After obtaining the polariza-

tion vectors, we can calculate the extinction cross section using

$$C_{\text{ext}} = \frac{4\pi k}{|\mathbf{E}_0|^2} \sum_{j=1}^{N} \text{Im}(\mathbf{E}_{\text{inc},j}^* \cdot \mathbf{P}_j).$$

For an infinite array of particles, a semi-analytical solution to Equation 3 was introduced^{19,61} for the wave vector perpendicular to the array axis (or plane), assuming the same induced polarization in each array element. This provides a simple way to analyze the coupling effects on the plasmon resonance line shape. The expression for the polarization of each particle reads as

$$P = \frac{\alpha_S E_0}{1 - \alpha_S S}$$
 and $C_{\text{ext}} = 4\pi Nk Im(P/E_0)$, 5

where the dimensionless quantity S is the retarded dipole sum given by

$$S = \sum_{j \neq i} \left[\frac{(1 - ikr_{ij})(3cos^2\theta_{ij} - 1)e^{ikr_{ij}}}{r_{ij}^3} + \frac{k^2sin^2\theta_{ij}e^{ikr_{ij}}}{r_{ij}} \right],$$

where θ_{ij} is the angle between r_{ij} and the polarization direction. The expression for S contains two terms. The first term has $1/r_{ij}^3$ and $1/r_{ij}^2$ dependence that contributes to short-range and intermediate-range interactions, while the second term with $1/r_{ij}$ (radiative dipolar interaction) contributes to long-range interactions. Each of these terms is modulated by an exponential factor, $e^{ikr_{ij}}$ that incorporates retardation effects into the results. The real part of S determines the shift in λ_{max} , where positive (negative) values correspond to red(blue)shifts. The imaginary part of S determines the linewidth of the resonance, where negative (positive) values give narrowed (broadened) line shapes compared to that of a single nanoparticle. To this end, analytical expressions for dipole sums for 1D arrays are also given by Markel. 23

Results and discussion

Plasmonic/photonic extinction line shapes are governed by several factors among which the interparticle spacings and the polarization and wave vector directions of the incident light are vital. To understand this, we consider an application to a 1D chain of 400 spherical silver nanoparticles (in vacuum) whose radii are 50 nm and we study the extinction efficiency (ratio of the extinction cross section to the total cross-sectional area of all the particles in the array). We consider the spectral range 300-650 nm for these calculations, and we choose the dielectric function from Johnson and Christy⁶² to describe the silver nanoparticles. Some of these calculations are similar to those presented in the original SLR work by Zou et al^{19,21} except that a different dielectric function was used there that is now considered less accurate than Johnson and Christy. Two situations are studied. In the first, the wave and polarization vectors are taken to be perpendicular to the array axis (see Figure 1 upper panel). Here, the interparticle spacings were fixed at certain values in the range 200-600 nm. The extinction spectrum of an individual particle is also plotted alongside as a guide to the eye. In the second set of calculations, the wave vector is parallel to the array axis, with the polarization perpendicular to it (see Figure 1 lower panel). In this case, the interparticle spacings range between 400 and 600 nm.

The upper panel shows a typical LSPR spectrum for the single silver particle, peaking near 396 nm. For the arrays, this broad LSPR peak is still present (but now slightly blueshifted from the single particle LSPR as it is the upper polariton mode). In addition, there is a sharp SLR peak at wavelengths that are shifted somewhat red from the RA wavelength, corresponding to the lower polariton mode. There is also a sharp dip in the extinction at a wavelength that matches the spacing due to the RA. As mentioned earlier, the SLR and LSPR peaks can be considered to be the lower and upper polariton modes in which light and plasmon excitation are coherently

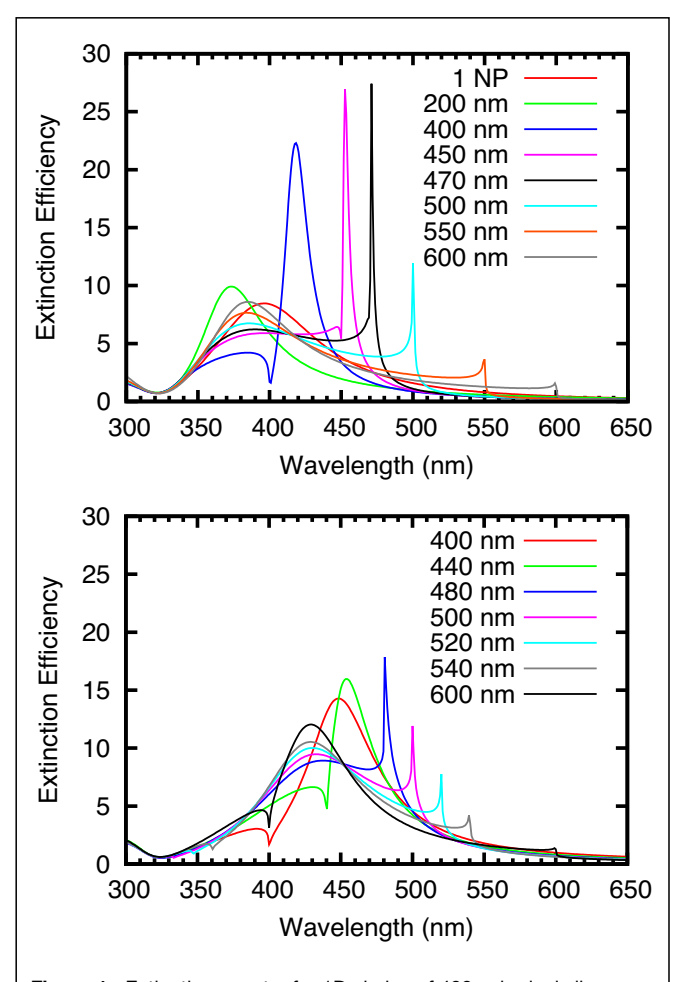


Figure 1. Extinction spectra for 1D chains of 400 spherical silver nanoparticles of radii 50 nm. The wave vector is chosen perpendicular (upper panel) and parallel (lower panel) to the array axis with the polarization perpendicular to it. The interparticle spacings are fixed at 200 nm, 400 nm, 450 nm, 470 nm, 500 nm, 550 nm, and 600 nm (upper panel) and 400 nm, 440 nm, 480 nm, 500 nm, 520 nm, 540 nm, and 600 nm (lower panel). The isolated single nanoparticle (NP) spectrum is also plotted alongside for comparison.

mixed. However, unlike the description that comes from low dimensional models like the Jaynes-Cummings model, where the uncoupled modes are replaced by the polaritonic modes, in this case we see that the RA (an uncoupled mode) can still be present even when the polaritonic modes are dominant. Note also that both the SLR and RA redshifts as the interparticle spacing in Figure 1 (upper panel) is increased, with the difference in wavelength decreasing, such that the RA merges with the SLR for spacings above 470 nm. The highest extinction efficiency (as determined by the ratio of cross section per particle to the geometrical area of the particle) is 27.4, as seen for the interparticle spacing of 470 nm. The sharp, dispersive peak for this spacing has a width of \sim 2 nm. The single nanoparticle LSPR has a width of \sim 86 nm and is centered at 396 nm, so we see that the SLR appears when the RA is to the red of the LSPR, and is much narrower than the SLR. In the lower panel, the highest extinction efficiency of

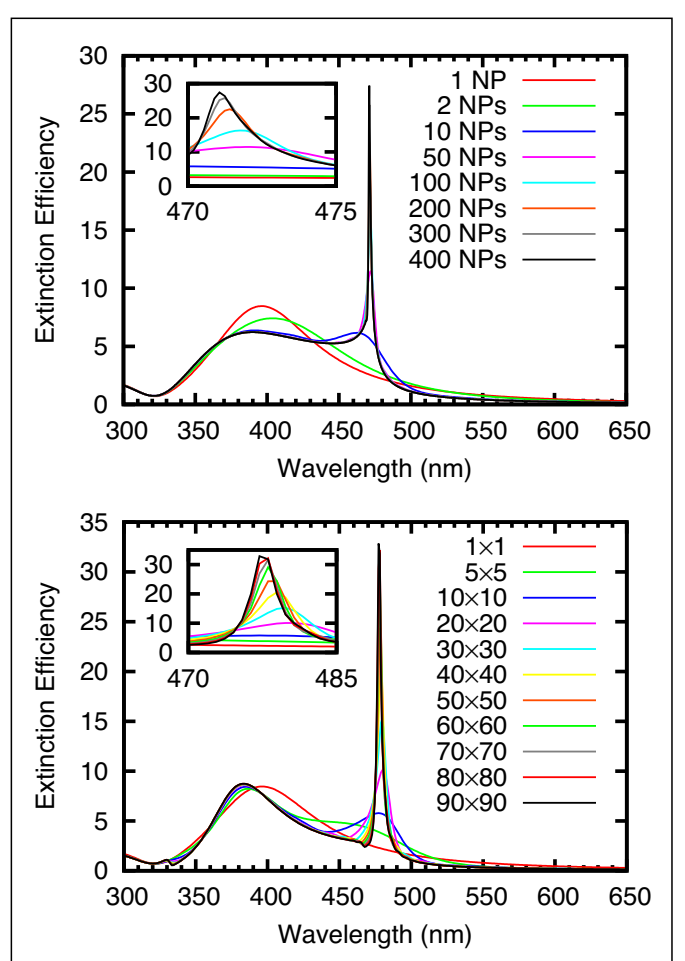


Figure 2. Extinction spectra of a 1D array (upper panel) and a 2D square array (lower panel) of spherical silver nanoparticles of radii 50 nm. The maximum number of nanoparticles (NPs) in the 1- and 2D arrays are 400 and 90×90 , respectively. The wave and polarization vectors are perpendicular to the array and the interparticle spacing is fixed at 470 nm in both cases. The insets highlight the blueshift of the plasmon wavelength as the array size increases.

17.9 is noted for an interparticle spacing of 480 nm. It has a width of ~ 8 nm. This SLR is also less intense compared to the former case, since the incident field oscillates along the array (leading to interference effects in the dipole sums) when the wave vector is parallel to the array, in contrast to having a constant field when the wave vector is perpendicular to the array. The RA appears at wavelengths 400 nm and 440 nm, which are the same wavelengths as in Figure 1 (upper).

The polarization response associated with the dipolar lattice plasmon and hence the extinction spectrum also depends on the size of the array. To that end, **Figure 2** (upper panel) depicts the extinction spectra of 1D chains of silver nanoparticles of radii 50 nm (in vacuum) for a fixed interparticle spacing of 470 nm with the wave and polarization vectors perpendicular to the array axis. The effect of number of particles in the array is revealed by gradually increasing the particles, starting from one up to 400. For smaller arrays (such as with 10 particles) a broad spectrum is noted, while the width of

the spectrum narrows down to ~ 15 nm with 50 particles, and it keeps on narrowing down further with increasing array size. This behavior arises because the induced dipoles are all aligned near the SLR maximum, and add constructively to the dipole sum in Equation 6. At the RA wavelength, all the $e^{ikr_{ij}}$ terms are unity and the dipole sum maximizes, while at the SLR wavelength there is phase cancellation involved such as to make the real part of $\alpha_S S$ as close to unity as possible. With 400 particles, we observe an extinction efficiency of 27.4 and a spectral width of \sim 2 nm. The sharper resonances indicate stronger induced optical frequency fields associated with the nanosystem, and in earlier work this was used to produce enhancements in SERS.³⁵ There is also a slight blueshift in the plasmon wavelength (see inset in Figure 2) as the number of particles is increased. This arises due to the larger dipole sum from the second term in Equation 6 for larger k values. 63 Figure 2 (lower panel) depicts the extinction efficiency of a finite 2D array where the number of particles is gradually increased to 90 particles in both directions. An extinction efficiency of 32.9 is noted for the 2D array compared to 27.4 for the 1D array. This suggests that 2D arrays can provide higher quality (Q) factors than 1D arrays; however, the line shape function for the 1D arrays is more complicated than this analysis suggests due to its cusp-like character. 23,64 Also note that the SLR peak is more redshifted in the 2D array ($\lambda = 477$ nm) compared to the 1D array ($\lambda = 471$ nm) due to the larger dipole sum. In the 2D array, the dip at $\lambda = 470$ nm corresponds to the RA. Note that the 2D array shows an additional RA dip at around $\lambda = 335$ nm (i.e., smaller by $1/\sqrt{2}$) due to scattering in the (1,1) lattice direction, as opposed to (1,0) and (0,1) scattering for the RA at 470 nm.

SLRs can also arise when the particle spacing is about half of the plasmon wavelength, as long as the polarization is parallel to the array. This is illustrated in **Figure 3** where the extinction spectra of a 1D chain of silver nanoparticles of radii 50 nm (in vacuum) is plotted for a fixed interparticle spacing of 260 nm. The polarization is perpendicular in this case (upper panel). Similar to Figure 2, the effect of number of particles in the array is significant. With 200 particles, we observe SLR behavior with a maximum extinction efficiency of 31.3 and a spectral width of \sim 5 nm. A gradual decrease in the peak extinction efficiency is noted as we increase the number of particles above 200, and there is a redshift in the SLR peak. In addition, a RA dip is observed at 520 nm, that is, at twice the interparticle spacing. These features are different from Figure 1 (lower panel) where the wave vector is also parallel, but the resonance condition is found when the interparticle spacing is approximately an integer multiple of the wavelength. In addition, if the wave vector is perpendicular to the array with spacing that is half the LSPR wavelength, there is no SLR peak (Figure 3 lower panel). This is because here the near field interactions between the dipoles nullify the SLR response. This reflects a factor of -1 in the interactions between adjacent dipoles originating from the $e^{ikr_{ij}}$ term in

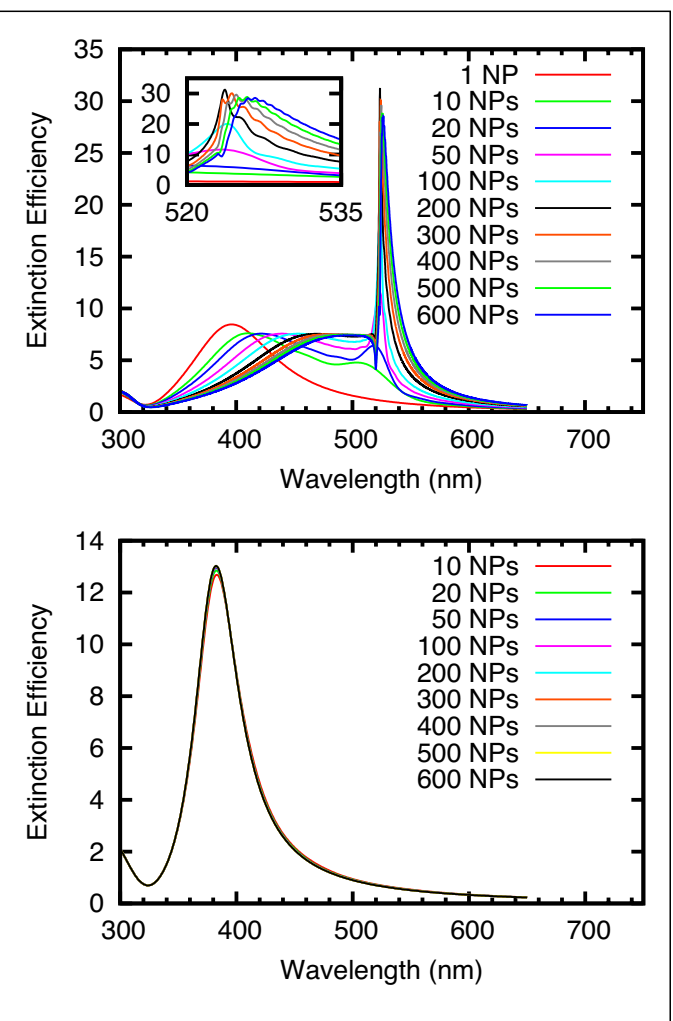


Figure 3. Extinction spectra of a 1D chain of spherical silver nanoparticles (NPs) of radius 50 nm. A maximum number of 600 particles are considered with the interparticle spacing fixed at 260 nm. The wave vector is chosen parallel (upper panel) and perpendicular (lower panel) to the array axis with the polarization perpendicular to it. The inset highlights the redshift of the plasmon wavelength as the array size increases.

Equation 6, and it contrasts with the parallel wave vector case where the incident field provides a second -1 factor so that intermediate field contributions are constructive.

The size of the nanoparticle also governs the plasmonic response of the array. **Figure 4** illustrates this for a 1D chain of 400 spherical silver nanoparticles (in vacuum) of radii 30 nm (upper panel) and 100 nm (lower panel). The wave and polarization vectors are chosen perpendicular to the chain axis. This is analogous to the situation in Figure 1 (upper panel) where 50 nm radii particles were considered. Here, the array spacings are varied ranging between 300 and 420 nm (for 30 nm radii particles) and between 400 and 1000 nm (for 100 nm radii particles). The plasmonic response of the array shifts to a narrow spectral range of 300–500 nm for the 30 nm radii and a broader spectral range of 300–1200 nm for the 100 nm radii. This is in comparison to the 300–650 nm spectral range for 50 nm radii particles as in

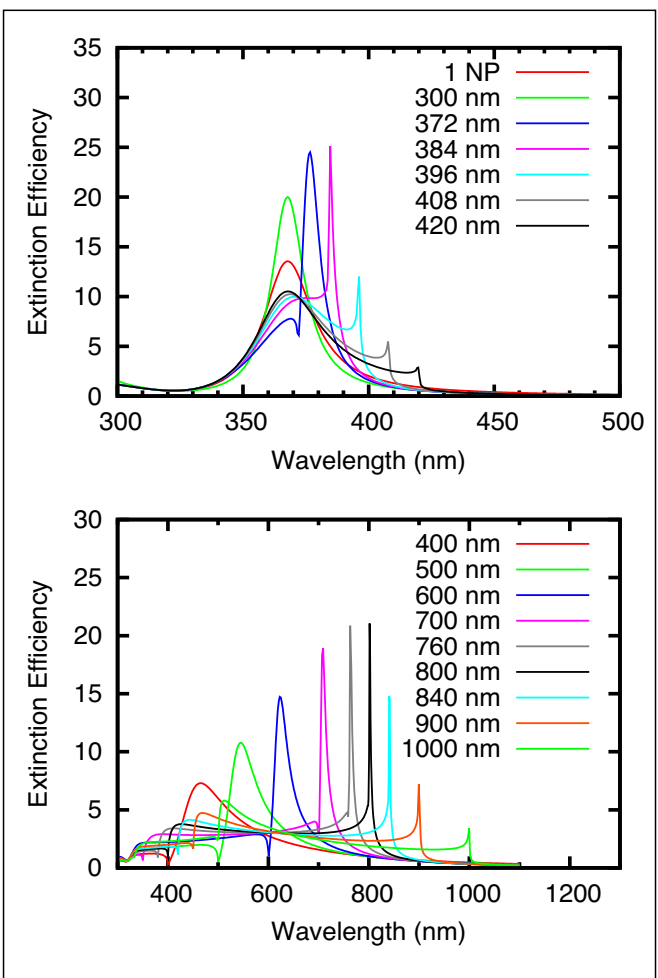


Figure 4. Extinction spectra of a 1D chain of spherical silver nanoparticles (NPs) similar to Figure 1 (upper panel), except now the radii are 30 nm (upper panel) and 100 nm (lower panel), respectively. The interparticle spacings are fixed at 300 nm, 372 nm, 384 nm, 396 nm, 408 nm, and 420 nm, respectively, for 30 nm radii, and are fixed at 400 nm, 500 nm, 600 nm, 700 nm, 760 nm, 800 nm, 840 nm, 900 nm, and 1000 nm, respectively, for 100 nm radii particles.

Figure 1. Comparing the upper and lower panels in Figure 4, we see that the previously discussed redshift in the dipole resonance with increased spacing spans a larger range of wavelengths for particles of larger radii. This is due to dynamic depolarization and radiative damping for individual particles, which redshifts and broadens the LSPRs as particle size increases. 65,66 Larger particles can also show higher multipole resonances to the blue of the dipole resonance, but these are not included in the coupled-dipole calculations. For the 30 nm radii particles, a highest extinction efficiency of 24.96 is noted for an interparticle spacing of 384 nm, while for 100 nm radii particles, a highest extinction efficiency of 21.1 is noted for an interparticle spacing of 800 nm. This is in comparison to an extinction efficiency of 27.4 for 50 nm radii particles with an interparticle spacing of 470 nm (see Figure 1). Another feature is that the 30 nm radii particles show slightly broader SLR peaks, that is, lower *Q*-factors, compared to 50 nm radii, and the 100 nm radii peak is also broader than for 50 nm. For example, for an interparticle spacing of 384 nm,

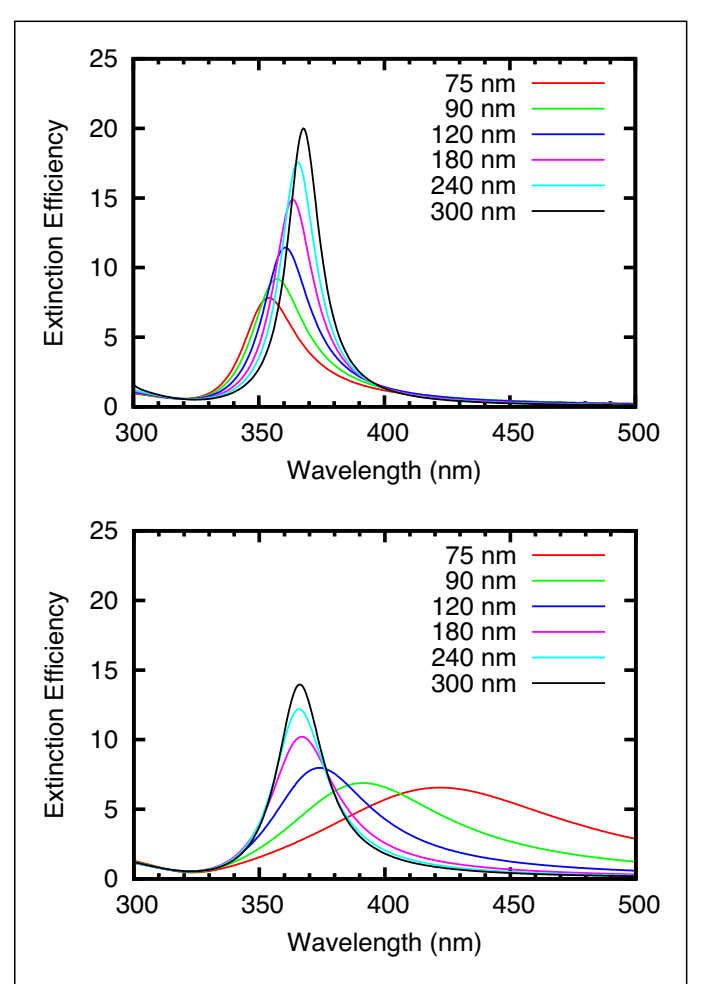


Figure 5. Extinction spectra of a 1D chain of spherical silver nanoparticles of radius 30 nm (in vacuum). The 1D array consists of 400 particles with the interparticle spacings fixed at 75 nm, 90 nm, 120 nm, 180 nm, 240 nm, and 300 nm, respectively. The wave vector is chosen perpendicular to the array axis while the polarization vector is perpendicular (upper panel) and parallel (lower panel) to it.

the plasmon resonance peaks at 384.6 nm and has a width of \sim 2.8 nm compared to 2.0 nm for the most intense peak for the 50 nm particle. For 100 nm radii particles, the most intense plasmon peak occurs at 801.7 nm for an interparticle spacing of 800 nm, and has a plasmon width of \sim 3.6 nm.

Figure 5 shows the extinction spectra of a 1D chain of 400 silver nanoparticles of radii 30 nm (in vacuum) with interparticle spacings fixed at certain values ranging between 75 and 300 nm. The wave vector is assumed perpendicular to the array axis, and we consider two scenarios: (1) the polarization vector perpendicular to the array axis (upper panel), and (2) the polarization vector parallel to the array axis (lower panel). Here, the wavelength range is chosen to be 300–500 nm, so these calculations consider wavelengths that include the LSPR, and where the RA is well to the red of the LSPR such that the LSPR mode is the lower polariton. However, the polaritonic coupling is extremely weak in this case so the redshift expected relative to the single particle resonance that is in Figure 4 (upper panel) is barely apparent

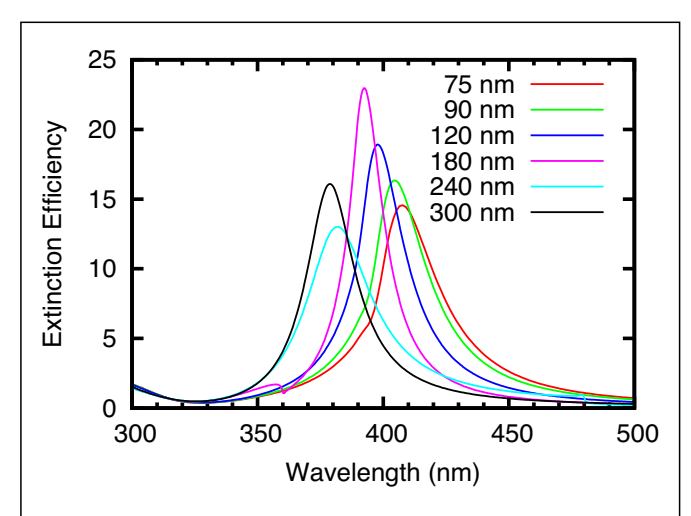


Figure 6. Extinction spectra of a 1D chain of spherical silver nanoparticles of radius 30 nm (in vacuum). The 1D array consists of 400 particles with interparticle spacings fixed at 75 nm, 90 nm, 120 nm, 180 nm, 240 nm, and 300 nm, respectively. The wave vector is chosen parallel to the array axis while the polarization vector is perpendicular to it.

in the 300 nm separation result (corresponding to the closest overlap of the RA and LSPR). However, the spacings considered here are such that near- and intermediate-field interactions can play a role. Indeed, the LSPR resonance that is near 370 nm for 300 nm spacing is blueshifted in the upper panel as spacing is decreased (a result that is similar to what was observed long ago^{19,61}) and redshifted in the lower panel. This is similar to effects found with H- and J-aggregates of dye molecules (where only near-field interactions are usually considered), where dipole alignment perpendicular to the array axis (H-aggregate) leads to blueshifted absorption spectra as the intermolecular coupling gets stronger, while alignment parallel to the axis (J-aggregates) leads to redshifted spectra. We also see that the plasmon in the upper panel gets dampened as it blueshifts while the lower panel shows the integrated intensity is higher but broadens as the spacing decreases. This behavior arises because the silver dielectric function becomes lossier in the blueshifted case, especially for wavelengths around 350 nm, while depolarization and radiative damping effects lead to broadening of the line shape in the redshifted case.

Figure 6 shows the extinction spectra of a one-dimensional chain of 400 silver nanoparticles of radii 30 nm (in vacuum) with interparticle spacings fixed at values smaller than the wavelength ranging between 75 and 300 nm (non-SLR case). In contrast to Figure 5, here we consider the wave vector parallel to the array. The polarization is perpendicular, so we compare Figure 5 (upper panel) with Figure 6. We see in Figure 6 that the plasmon redshifts with decreasing separation, which is the opposite result to Figure 5 (upper panel). This is because although dipole alignment is perpendicular to the axis, the parallel wave vector in combination with a

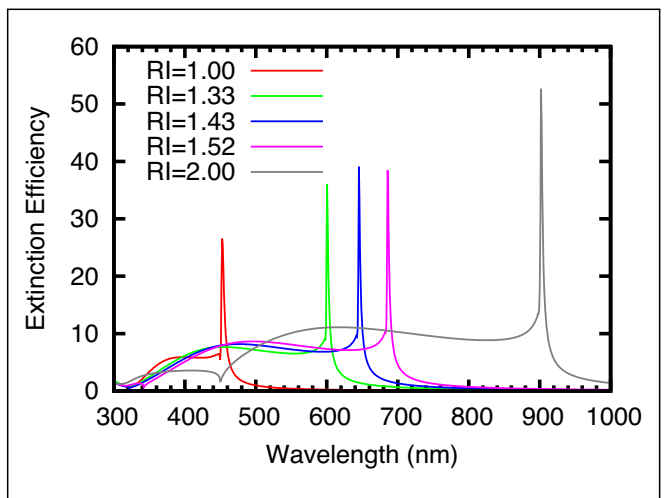


Figure 7. Extinction spectra of a 1D chain of spherical silver nanoparticles of radii 50 nm similar to Figure 1 (upper panel), but in the presence of different surrounding medium as indicated by their refractive indices (RIs). The wave and polarization vectors are perpendicular to the array and the interparticle spacing is fixed at 450 nm.

plasmon wavelength that is a few times larger than the spacing causes the dipoles to slowly oscillate in sign along the array. This leads to a combination of attractive and repulsive interactions that are dominated by the attractive interactions in this case.

Similar to individual plasmonic nanoparticles, 8,9,67 nanoparticle arrays that support SLRs are also sensitive to changes in the refractive index (RI) of the surrounding medium. Figure 7 shows the extinction spectra of 1D chains of 400 spherical silver nanoparticles of radii 50 nm where the wave and polarization vectors are perpendicular to the array axis and the interparticle spacing is fixed at 450 nm. We considered a series of background refractive indices that correspond to air (RI = 1.00), water (RI = 1.33), organic molecules (RI = 1.43), common solvents (RI = 1.52), and high-index materials (RI = 2.00). The SLR peak is found to gradually shift to longer wavelengths for higher indices. This is not surprising given that the diffraction wavelength is proportional to the RI. There is also a redshift in the broad LSPR peak with increasing RI (also not surprising), and this makes it possible to have high intensity SLRs at 900 nm, in contrast to the sharp cutoff in SLR intensity that we see around 600 nm in the vacuum case in Figure 1 (upper panel). Another feature of Figure 7 is that there is a RA dip at 450 nm for RI = 2.0 (and similar dips at half the SLR wavelengths in the other curves, but harder to see). This corresponds to RAs associated with the second harmonic diffraction, which is an effect that is included in the coupled-dipole method due to the nonlinear frequency dependence of the dipole interaction in Equation 2. This result is related to past work on plasmon-enhanced second harmonic diffraction⁶⁸ but no SLR is seen for RI = 2.0 near 450 nm as the hyperpolarizability response in the induced polarization is not included in Equation 1.

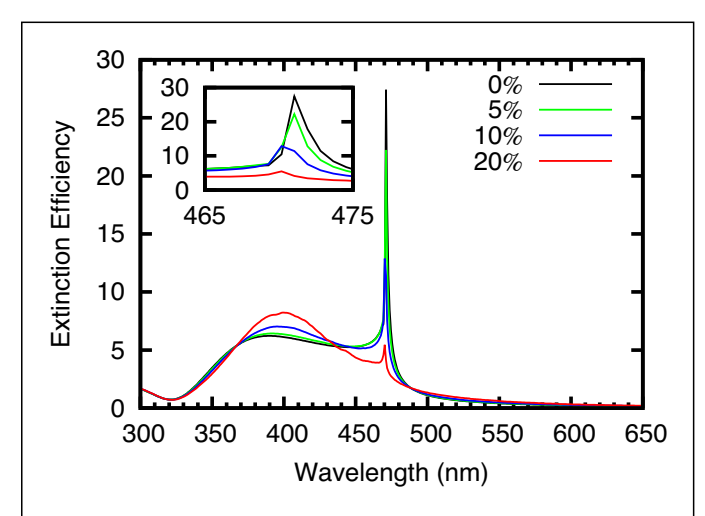


Figure 8. Extinction spectra of a 1D chain of spherical silver nanoparticles of radii 50 nm at an interparticle spacing of 470 nm (similar to Figure 1) but with positional disorder having different disorder amplitudes. The wave and polarization vectors are perpendicular to the array.

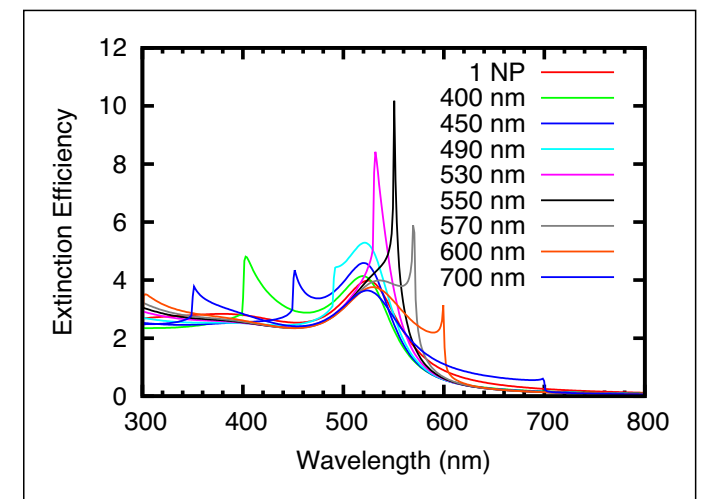


Figure 9. Extinction spectra of a 1D chain of spherical gold nanoparticles (NPs) similar to Figure 1. The interparticle spacings are fixed at 400 nm, 450 nm, 490 nm, 530 nm, 550 nm, 570 nm, 600 nm, and 700 nm, respectively.

Advances in lithography techniques have enabled the fabrication of nanoparticle arrays with a high degree of periodicity. However, if the array spacings deviate from a perfect lattice, the linewidth and intensity of the lattice resonance are affected. As a result, the effect of array disorder on SLRs can be important. This is illustrated in **Figure** 8 where we considered a 1D chain of 400 spherical silver nanoparticles of radii 50 nm. The incident wave and polarization vectors are chosen perpendicular to the array axis. Here, we start with a perfect lattice with interparticle spacing of 470 nm (0% disorder) as in Figure 1 (upper panel), and then deviations from a perfect lattice are considered. This is achieved by the inclusion of position perturbations of different amplitudes

to the unperturbed nanoarray with gaussian-distributed random displacements corresponding to standard deviations of 5%, 10%, and 20%, respectively. The sharp extinction peak with peak intensity of 27.4 for the perfect lattice gradually decreases to 22.2, 12.8, and 5.4 as the array disorder increases to 5%, 10%, and 20%, respectively. The SLR peak also gets slightly blueshifted due to the disorder that results in a weaker interaction between the particles and thereby leads to the quenching of the dipole sum.

The plasmonic response of an array also depends on the element that each nanoparticle is made up of. To study this, we consider a 1D chain of 400 nm spherical gold nanoparticles of radii 50 nm (in vacuum) in Figure 9 analogous to Figure 1. The wavelength-dependent optical constants of gold are again taken from Johnson and Christy.⁶² The wave and polarization vectors are chosen perpendicular to the array axis and the interparticle spacing is fixed at values ranging between 400 and 700 nm. The extinction spectrum of an individual gold nanoparticle (which shows a typical LSPR peak near 520 nm) is also plotted as a guide to the eye. In this case, we see that the SLR spectra for gold extend up to 700 nm, but are otherwise similar to silver for wavelengths above 520 nm. The highest extinction efficiency of 10.2 is noted for an interparticle spacing of 550 nm. This is weak in comparison to the analogous silver case. The width of the peak is \sim 8.4 nm. We also see RA response for interparticle spacings of 400 nm, 450 nm, and 490 nm, but in contrast to silver, these RAs show up as peaks rather than as dips. This change arises because the dielectric response of gold at short wavelengths (below 500 nm) is dominated by interband transitions, rather than plasmon excitation, such that the polarizability of gold has a positive real part in this wavelength range, in contrast to the negative real part for silver.

Conclusion

In this Review, we have used the coupled-dipole method to study the electrodynamics of 1D and 2D arrays of silver and gold nanoparticles, with an emphasis on the properties of LSPRs, SLRs, and RAs as a function of array structural properties (lattice spacing and number of particles, of nanoparticle radius, of refractive index, and of the direction of the incident wave and polarization vectors of light). In addition, we have interpreted the results in terms of the physical mechanisms that determine the variation of LSPR and SLR resonant frequencies and widths with lattice spacing for different choices of array structures and incident light properties. The coupled-dipole method is not capable of describing the contributions from higher-order multipolar LSPRs to the array properties, but previous studies have demonstrated that higher-order multipoles do not influence the radiative coupling for particles of radii 50 nm or smaller, provided they are separated by half the wavelength or more, 19,27 which is almost always the case in what we considered. However, for relatively large nanoparticles



multipolar LSPRs can play a role, as has occasionally been found. ⁶⁹ In this case it is possible to use the coupled multipole or finite-difference time-domain (FDTD) methods to study the arrays, but for carrying out a broad survey such as has been done in this Review, the coupled-dipole method is extremely useful. Almost all the experimental studies of particle arrays have been done for 2D arrays; one exception is the work by Törmä and co-workers on 1D arrays. ⁷⁰ However, we have demonstrated that the 1D arrays of most interest to this article often give results that are similar to 2D arrays, but subject to important differences in array symmetry and photonic band structure effects.

Acknowledgments

We thank M. Bourgeois for valuable discussions with the SLRpy code.

Author contributions

D.D. assisted in manuscript development, performed all the calculations and writing of the manuscript. G.C.S. led the manuscript development and worked with D.D. on writing of the manuscript.

Funding

The authors acknowledge financial support through the US Department of Energy, Office of Basic Energy Sciences, under Grant No. DE-SC0004752 (for methods development) and the National Science Foundation, Division of Materials Research, under Grant No. DMR-2207215 (applications).

Conflict of interest

On behalf of all authors, the corresponding author states that there is no conflict of interest.

References

- 1. M. Faraday, Philos. Trans. R. Soc. Lond. 147, 145 (1857)
- 2. R. Jin, Y. Wei, C.A. Mirkin, K.L. Kelly, G.C. Schatz, J.G. Zheng, Science 294, 1901 (2001)
- 3. M.L. Brongersma, Nat. Mater. 2, 296 (2003)
- 4. E. Ozbay, Science 311, 189 (2006)
- 5. A.F. Koenderink, A. Alù, A. Polman, Science 348, 516 (2015)
- 6. A.I. Fernández-Domínguez, F.J. García-Vidal, L. Martín-Moreno, *Nat. Photonics* 11, 8 (2017)
- 7. U. Kreibig, M. Vollmer, Optical Properties of Metal Clusters (Springer, Berlin, 1995)
- 8. C.L. Haynes, R.P. Van Duyne, J. Phys. Chem. B 105, 5599 (2001)
- 9. K.L. Kelly, E. Coronado, L.L. Zhao, G.C. Schatz, J. Phys. Chem. B 107, 668 (2003)
- 10. F. Wang, Y.R. Shen, Phys. Rev. Lett. 97, 206806 (2006)
- 11. W.A. Murray, W.L. Barnes, Adv. Mater. 19, 3771 (2007)
- 12. K.A. Willets, R.P. Van Duyne, Annu. Rev. Phys. Chem. 58, 267 (2007)
- 13. V. Giannini, A.I. Fernández-Domínguez, S.C. Heck, S.A. Maier, *Chem. Rev.* 111, 3888 (2011)
- 14. Y. Chu, E. Schonbrun, T. Yang, K.B. Crozier, Appl. Phys. Lett. 93, 181108 (2008)
- 15. K.M. Mayer, J.H. Hafner, *Chem. Rev.* 111, 3828 (2011)
- 16. E. Prodan, C. Radloff, N.J. Halas, P. Nordlander, Science 302, 419 (2003)
- 17. K.-H. Su, Q.-H. Wei, X. Zhang, J.J. Mock, D.R. Smith, S. Schultz, *Nano Lett.* **3**, 1087 (2003)
- 18. L. Gunnarsson, T. Rindzevicius, J. Prikulis, B. Kasemo, M. Käll, S. Zou, G.C. Schatz, J. Phys. Chem. B 109, 1079 (2005)
- 19. S. Zou, N. Janel, G.C. Schatz, J. Chem. Phys. 120, 10871 (2004)
- 20. S. Zou, G.C. Schatz, Chem. Phys. Lett. 403, 62 (2005)

- 21. V.G. Kravets, F. Schedin, A.N. Grigorenko, Phys. Rev. Lett. 101, 087403 (2008)
- 22. K.T. Carron, W. Fluhr, M. Meier, A. Wokaun, H.W. Lehmann, *J. Opt. Soc. Am. B* 3, 430 (1986)
- 23. V.A. Markel, J. Mod. Opt. 40, 2281 (1993)
- 24. B. Auguié, W.L. Barnes, Phys. Rev. Lett. 101, 143902 (2008)
- 25. E.M. Hicks, S. Zou, G.C. Schatz, K.G. Spears, R.P. Van Duyne, L. Gunnarsson, T. Rindzevicius, B. Kasemo, M. Käll, *Nano Lett.* **5**, 1065 (2005)
- 26. W. Zhou, T.W. Odom, Nat. Nanotechnol. 6, 423 (2011)
- 27. B. Lamprecht, G. Schider, R.T. Lechner, H. Ditlbacher, J.R. Krenn, A. Leitner, F.R. Aussenegg, *Phys. Rev. Lett.* **84**, 4721 (2000)
- 28. M.B. Ross, C.A. Mirkin, G.C. Schatz, J. Phys. Chem. C 120, 816 (2016)
- 29. V.G. Kravets, A.V. Kabashin, W.L. Barnes, A.N. Grigorenko, *Chem. Rev.* **118**, 5912 (2018) 30. W. Wang, M. Ramezani, A.I. Väkeväinen, P. Törmä, J.G. Rivas, T.W. Odom, *Mater. Today* **21**, 303 (2018)
- 31. W. Zhou, M. Dridi, J.Y. Suh, C.H. Kim, D.T. Co, M.R. Wasielewski, G.C. Schatz, T.W. Odom, *Nat. Nanotechnol.* **8**, 506 (2013)
- 32. A. Fernandez-Bravo, D. Wang, E.S. Barnard, A. Teitelboim, C. Tajon, J. Guan, G.C. Schatz, B.E. Cohen, E.M. Chan, P.J. Schuck, T.W. Odom, *Nat. Mater.* **18**, 1172 (2019) 33. D.C. Hooper, C. Kuppe, D. Wang, W. Wang, J. Guan, T.W. Odom, V.K. Valev, *Nano Lett.* **19**, 165 (2019)
- 34. L.L. Zhao, K.L. Kelly, G.C. Schatz, J. Phys. Chem. B 107, 7343 (2003)
- 35. S. Zou, G.C. Schatz, J. Chem. Phys. 121, 12606 (2004)
- 36. S. Zou, G.C. Schatz, Phys. Rev. B 74, 125111 (2006)
- 37. S. Zou, G.C. Schatz, Nanotechnology 17, 2813 (2006)
- 38. A. Yang, T.B. Hoang, M. Dridi, C. Deeb, M.H. Mikkelsen, G.C. Schatz, T.W. Odom, *Nat. Commun.* **6**, 6939 (2015)
- 39. D. Wang, A. Yang, A.J. Hryn, G.C. Schatz, T.W. Odom, *ACS Photonics* 2, 1789 (2015) 40. A. Yang, A.J. Hryn, M.R. Bourgeois, W.-K. Lee, J. Hu, G.C. Schatz, T.W. Odom, *Proc. Natl. Acad. Sci. U.S.A.* 113, 14201 (2016)
- 41. J. Liu, W. Wang, D. Wang, J. Hu, W. Ding, R.D. Schaller, G.C. Schatz, T.W. Odom, *Proc. Natl. Acad. Sci. U.S.A.* **116**, 5925 (2019)
- 42. A.D. Sample, J. Guan, J. Hu, T. Reese, C.R. Cherqui, J.-E. Park, F. Freire-Fernández, R.D. Schaller, G.C. Schatz, T.W. Odom, *Nano Lett.* 21, 7775 (2021)
- 43. S.A. Maier, M.L. Brongersma, P.G. Kik, S. Meltzer, A.A.G. Requicha, H.A. Atwater, *Adv. Mater.* 13, 1501 (2001)
- 44. S.A. Maier, P.G. Kik, H.A. Atwater, S. Meltzer, E. Harel, B.E. Koel, A.A.G. Requicha, *Nat. Mater.* 2, 229 (2003)
- 45. S.A. Maier, P.G. Kik, H.A. Atwater, Phys. Rev. B 67, 205402 (2003)
- 46. D.S. Citrin, *Nano Lett.* **4**, 1561 (2004)
- 47. S.A. Maier, H.A. Atwater, J. Appl. Phys. 98, 011101 (2005)
- 48. L.A. Sweatlock, S.A. Maier, H.A. Atwater, J.J. Penninkhof, A. Polman, *Phys. Rev. B* 71, 235408 (2005)
- 49. D.S. Citrin, *Nano Lett.* **5**, 985 (2005)
- 50. S.R.K. Rodriguez, A. Abass, B. Maes, O. T. A. Janssen, G. Vecchi, J. Gómez Rivas, *Phys. Rev. X* 1, 021019 (2011)
- 51. S.R.K. Rodriguez, M.C. Schaafsma, A. Berrier, J. Gómez Rivas, *Phys. B* **407**, 4081 (2012)
- 52. A.D. Humphrey, W.L. Barnes, *Phys. Rev. B* **90**, 075404 (2014)
- 53. M.J. Huttunen, K. Dolgaleva, P. Törmä, R.W. Boyd, *Opt. Express* 24, 28279 (2016)
- 54. R. Guo, T.K. Hakala, P. Törmä, *Phys. Rev. B* **95**, 155423 (2017)
- 55. T.K. Hakala, H.T. Rekola, A.I. Väkeväinen, J.-P. Martikainen, M. Nečada, A.J. Moilanen, P. Törmä, *Nat. Commun.* **8**, 13687 (2017)
- 56. T.K. Hakala, A.J. Moilanen, A.İ. Väkeväinen, R. Guo, J.-P. Martikainen, K.S. Daskalakis, H.T. Rekola, A. Julku, P. Törmä, *Nat. Phys.* **14**, 739 (2018)
- 57. S. Deng, R. Li, J.-E. Park, J. Guan, P. Choo, J. Hu, P.J.M. Smeets, T.W. Odom, *Proc. Natl. Acad. Sci. U.S.A.* **117**, 23380 (2020)
- 58. R.K. Yadav, M. Otten, W. Wang, C.L. Cortes, D.J. Gosztola, G.P. Wiederrecht, S.K. Gray, T.W. Odom, J.K. Basu, *Nano Lett.* **20**, 5043 (2020)
- A.K. Boddeti, J. Guan, T. Sentz, X. Juarez, W. Newman, C. Cortes, T.W. Odom, Z. Jacob, Nano Lett. 22, 22 (2022)
- 60. J.M. McMahon, G.C. Schatz, S.K. Gray, *Phys. Chem. Chem. Phys.* **15**, 5415 (2013) 61. C.L. Haynes, A.D. McFarland, L.L. Zhao, R.P. Van Duyne, G.C. Schatz, L. Gunnars-
- son, J. Prikulis, B. Kasemo, M. Käll, J. Phys. Chem. B 107, 7337 (2003)
- 62. P.B. Johnson, R.W. Christy, Phys. Rev. B 6, 4370 (1972)
- 63. C. Cherqui, M.R. Bourgeois, D. Wang, G.C. Schatz, Acc. Chem. Res. 52, 2548 (2019)
- 64. S. Zou, G.C. Schatz, J. Chem. Phys. 122, 097102 (2005)
- 65. E.J. Zeman, G.C. Schatz, J. Phys. Chem. 91, 634 (1987)
- 66. M.B. Ross, G.C. Schatz, J. Phys. D 48, 184004 (2015)
- 67. E. Ringe, J.M. McMahon, K. Sohn, C. Cobley, Y. Xia, J. Huang, G.C. Schatz, L.D. Marks, R.P. Van Duyne, *J. Phys. Chem. C* 114, 12511 (2010)
- 68. A.C.R. Pipino, R.P. Van Duyne, G.C. Schatz, Phys. Rev. B 53, 4162 (1996)



PLASMONIC SURFACE LATTICE RESONANCES IN NANOPARTICLE ARRAYS

69. R. Li, M.R. Bourgeois, C. Cherqui, J. Guan, D. Wang, J. Hu, R.D. Schaller, G.C. Schatz, T.W. Odom, *Nano Lett.* **19**, 6435 (2019)

70. H.T. Rekola, T.K. Hakala, P. Törmä, ACS Photonics 5, 1822 (2018)

Publisher's Note

Springer Nature remains neutral with regard to jurisdictional claims in published maps and institutional affiliations.

Springer Nature or its licensor (e.g. a society or other partner) holds exclusive rights to this article under a publishing agreement with the author(s) or other rightsholder(s); author self-archiving of the accepted manuscript version of this article is solely governed by the terms of such publishing agreement and applicable law.